scientific reports

Check for updates

OPEN

Analysis of dynamic levitation process of the particle chain in a nonlinear standing wave field

Yaxing Wang✉, Liqun Wu, Linan Zhang, Hongcheng Wang, Guanwu Wu & Jiaxin Wu

This research delves into the dynamic behavior of acoustic levitation of the particle chain in a nonlinear standing wave field. Experimental acoustic levitation control tests reveal bifurcation and jump phenomena during dynamic adjustments to resonant cavity height. Employing the 10-particle chain experiments and the COMSOL simulation models, the Sine-Gordon 2D vibration model is established to study the dynamic deformation process of the particle chain. The study uncovers the nonlinear interaction of particle lateral vibrations, horizontal acoustic radiation force, and conical wave fields that generate the jumping standing wave field. Notably, the fourth particle acts as a prominent jumping critical point in the secondary standing wave field, facilitating the derivation of the particle chain's nonlinear levitation dynamics. This discovery provides us with a new method to regulate the particle chain system.

Keywords Particle chain, Acoustic levitation, Bifurcation, Jump, Sine-Gordon, Nonlinear standing wave field

The mechanism of an acoustic standing wave levitation is to use the nonlinear effect of high frequency acoustic wave[1] to produce the acoustic radiation force of standing wave field[2] to overcome the gravity, which is very important for semiconductor chips[3], cell manipulation[4], biomedicine[5], containerless transportation[6,7]. In terms of levitation effectiveness, the existing researches reveal the capability to not only arrange the dust particles into a ring pattern within the standing wave glass tube[8], but also suspend single or multiple particles of divers materials and sizes[9]; from the perspective of manipulation technology, it can capture[10], translate[11] and rotate particles[12], with uni-axial[7,13], multi-axis[14,15] and phase array manipulation[16]; from the theoretical research, the acoustic radiation force[17], the acoustic field pressure[18], the half-wavelength theory[17], the potential well equation[13,16], the vibration equation[19] and various motion equations[4,15] are obtained, and the height of the resonant cavity is also adjusted[3,11].

The current research on the dynamic levitation motion analysis of the particle chain is rare, and most of them are limited to steady-state analysis. However, in this paper, by dynamically adjusting the height of the resonant cavity, the bifurcation[20] and jump[21] phenomena of the particle chain in motion are found. In order to further verify these experimental phenomena, we constructed the corresponding theoretical model and simulation model, and conducted in-depth research. This paper focuses on the nonlinear interaction between the secondary acoustic radiation force[22] and lateral vibration of the dynamic particle chain and the conical standing wave field under the standing wave acoustic field, thus revealing the formation mechanism of the jumping standing wave field and obtaining the law of the nonlinear levitation change of the particle chain.

It is worth mentioning that the research in this paper finds that within a certain range of the resonant cavity, we can realize the overall control, fixed-point separation and delivery of the particle chain. Compared with the traditional phased array control method, this method has faster adjustment speed, better flexibility, less computation and higher control efficiency. This finding provides strong support for the promotion and optimization of the dynamic levitation motion of the particle chain in practical applications. In summary, the research in this paper not only reveals the complexity and diversity of the dynamic levitation motion of the particle chain, but also provides new ideas and methods for future research and application.

Results

(1) We use the single-axis standing wave field to suspend the particles, and realize the particle chain levitation and complex motion of the single-axis standing wave field by changing single or multiple conditions. The experimental results show that the dynamic levitation process of the 10-particle chain occurs under the condition of changing the height of the resonant cavity. From the initial state to the single pendulum motion, to

School of Mechanical Engineering, Hangzhou Dianzi University, Hangzhou 310018, China. ✉email: faywinter@126.com

the obvious bifurcation state and jump phenomenon, and finally to the initial state one by one, the process has good maneuverability and repeatability. The specific phenomena are as follows.

In this paper, the polystyrene particles with a density of 0.01 ~ 0.03 g/cm and a diameter of 2 mm were selected. The frequency of the ultrasonic generator is $f = 28$ kHz, and the acoustic velocity in the air is $v = 343$ m/s. The wavelength is calculated to be $\lambda = v/f = 12.25$ mm, and the half-wavelength is 6.125 mm.

The height of the initial state in Fig. 1a is denoted as H1, and the height of the bifurcation state in Fig. 1c is denoted as H2. The average values of H1 and H2 are obtained by repeated experiments: the average value of H1 is 67.48 mm, which is close to the theoretical 11 times and a half wavelength (67.375 mm). The average value of H2 is 69.23 mm, which is close to the theoretical 11.25 times half wavelength (68.906 mm), which is related to the subsequent simulation.

(2) In order to show the change of acoustic wave more intuitively, the ripple method is used to observe the waveform of the initial state and the waveform of the bifurcation state. The number of suspended particles is the state of no particles, the fourth particles and the 10-particle chain, respectively. The obvious change of the waveform can be seen, and the specific analysis is as follows in Fig. 2.

(3) Next, this paper uses COMSOL Multiphysics 6.1 to draw a two-dimensional model of a single-axis standing wave acoustic field. Based on the "pressure acoustics, frequency domain (acpr)" module, the height change of the resonant cavity of the standing wave acoustic field is simulated, and the distribution of acoustic pressure and standing wave nodes of the acoustic field at different resonant cavity heights is analyzed.

The acoustic wave model diagram of the conical standing wave field is established, and the single-axis standing wave field is simulated and analyzed by COMSOL. As shown in Fig. 3, the suspended particles at the wave nodes of the acoustic field form a conical standing wave levitation acoustic field of the 10-particle chain.

By adjusting the height of the resonant cavity, when the distance of the standing wave field is not an integer multiple of the half wavelength, the wave node begins to deform, the central wave node of each particle will split into two horizontal wave nodes, causing the suspended particle at the center to vibrate laterally due to the acoustic radiation force of the two horizontal wave nodes. When the distance increases by λ/8, the wave node deforms at both ends, as shown in Fig. 4. When the transverse distance between the two horizontal wave nodes is not large enough, the particles still do lateral vibration in the central position without jumping; when the distance is large enough, the particles can jump to the wave node at one end and maintain the position, which explains that the upper four particles do not bifurcate in the experiment, but the below six particles do, and the lateral vibration of the fourth particle is more intense as the jumping critical point.

The simulation height comes to 11 times the half-wavelength height (the 10-particle chain) on the test photo, as shown in Fig. 5. The simulation results are as follows: the simulation Fig. 5a is consistent with the experimental Fig. 1a, and the vertical levitation is stable at this time; the simulation Fig. 5b is consistent with the experimental Fig. 1b, and the single pendulum motion is occurred; the simulation Fig. 5c is consistent with the experimental Fig. 1c, and obvious bifurcation begins at this time. The simulation Fig. 5d–f and the experimental Fig. 1d–f are consistent. At this time, the vertical levitation position is gradually restored from the bifurcation, and finally to the initial state one by one, the process has good maneuverability and repeatability.

The acoustic pressure of the center and the bifurcation area before and after the bifurcation of the acoustic field is analyzed. As shown in Fig. 6, from the initial state to the bifurcation state, the central green line decreases sharply from the stable state, and the bifurcation blue line increases sharply from small to large, and then the waveform gradually returns to stability.

The reason for the generation of the jumping standing wave field is the horizontal acoustic radiation force generated by the lateral vibration of particles, which interacts with the original standing wave field to produce a secondary standing wave field. The reason is as shown in Fig. 7. It is found that the fourth particle is more intense as the jumping critical point. Therefore, only the fourth particle is analyzed in the simulation which effect is more obvious, resulting in a jump standing wave field in the horizontal direction, which makes the particle jump quickly. The secondary standing wave field in this paper is mainly caused by lateral vibration, and from the comparison of the influence diagrams of scattering amplitude, it shows minimal correlation with scattering, so the specific solution for the impact of scattering is not pursued, and only qualitative simulation analysis is conducted.

Discussion

Firstly, in the standing wave field, the acoustic levitation force and interaction forces between particles in the particle chain together constitute the basis of the nonlinear motion of the particle chain. The delicate balance and interaction between these forces make the motion of the particle chain exhibit rich and complex nonlinear characteristics.

Secondly, the adjustment of the resonant cavity height has a significant effect on the acoustic pressure and acoustic radiation force of the standing wave acoustic field. This effect is not only reflected in the change of the nature of the acoustic field itself, but also plays a key role in the nonlinear motion of the particle chain. The interaction force between the particles and the comprehensive force of these external fields are intertwined, which together determine the dynamic behavior of the particle chain.

Finally, the lateral jump phenomenon caused by the sudden change of the acoustic field is rooted in the interaction between the horizontal acoustic radiation force generated by the lateral vibration of all particles, and the lateral vibration of the fourth particle is more intense as the jumping critical point, resulting in the horizontal direction of the particle chain and the jump standing wave field. This process essentially reflects the transformation of the acoustic field from linear motion to nonlinear motion, that is, from single pendulum motion to nonlinear motion with soliton characteristics.

The research in this article not only enriches our understanding of the interaction between acoustic field and particle chain, but also provides a new perspective and idea for further research in related fields. This greatly

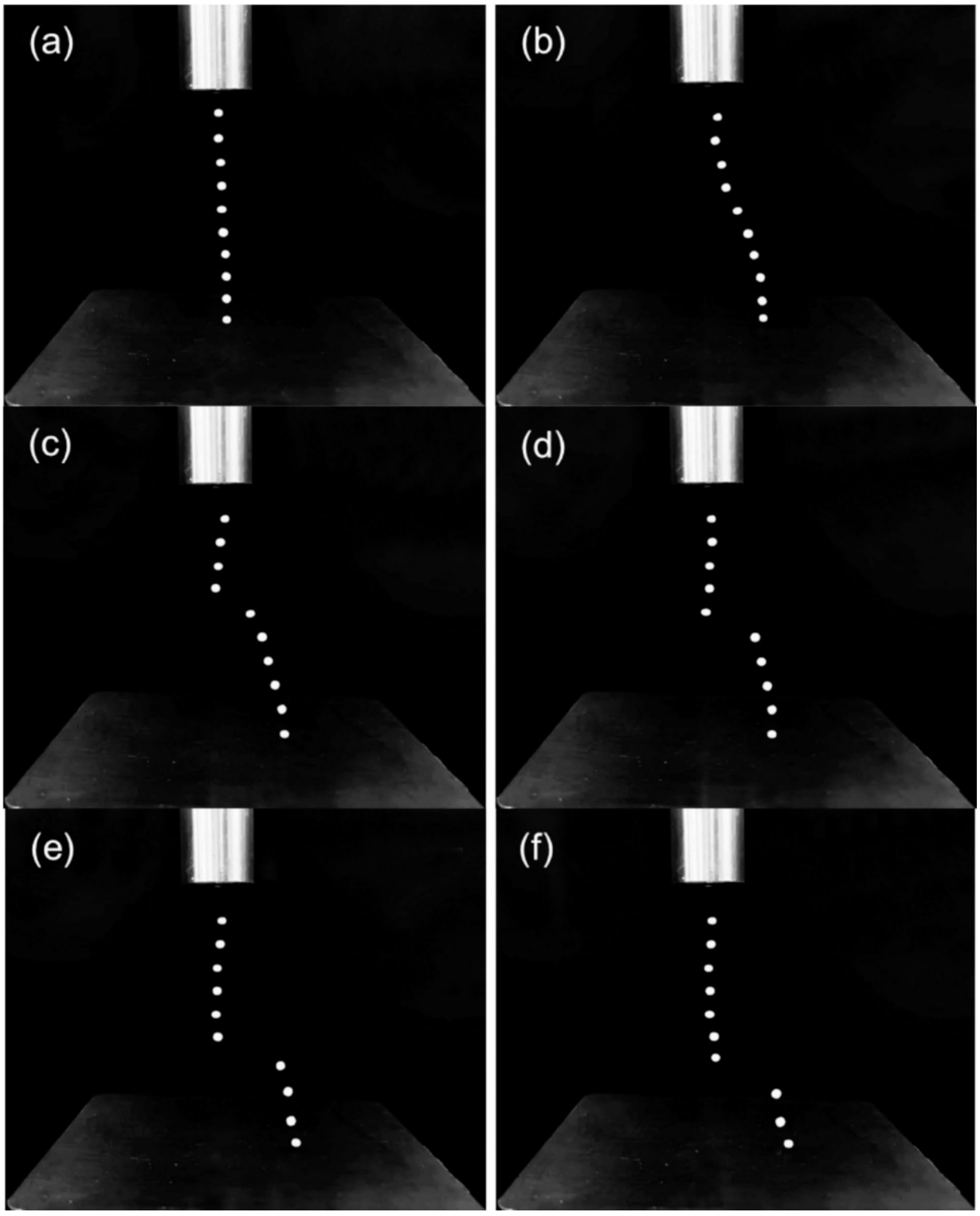

Fig. 1. Dynamic levitation process of the 10-particle chain in a standing wave field. **a** The stable suspended vertical particle chain, which can be called the initial state. **b** When the standing wave emission end is pulled up vertically and uniformly, the movement of the particle chain first undergoes the initial single pendulum motion. **c** When the height of the resonant cavity reaches λ/8 in a half-wavelength, the acoustic field jumps and bifurcation occurs. It can be seen that there is no obvious bifurcation in the above four particles, while the following six particles jump rapidly. **d**–**f** After the bifurcation occurs, the particle chain continues to be raised until the next half wavelength. At this time, the particle chain gradually returns to the vertical levitation state, and the bifurcated particles can jump back to the center position one by one from the fifth.

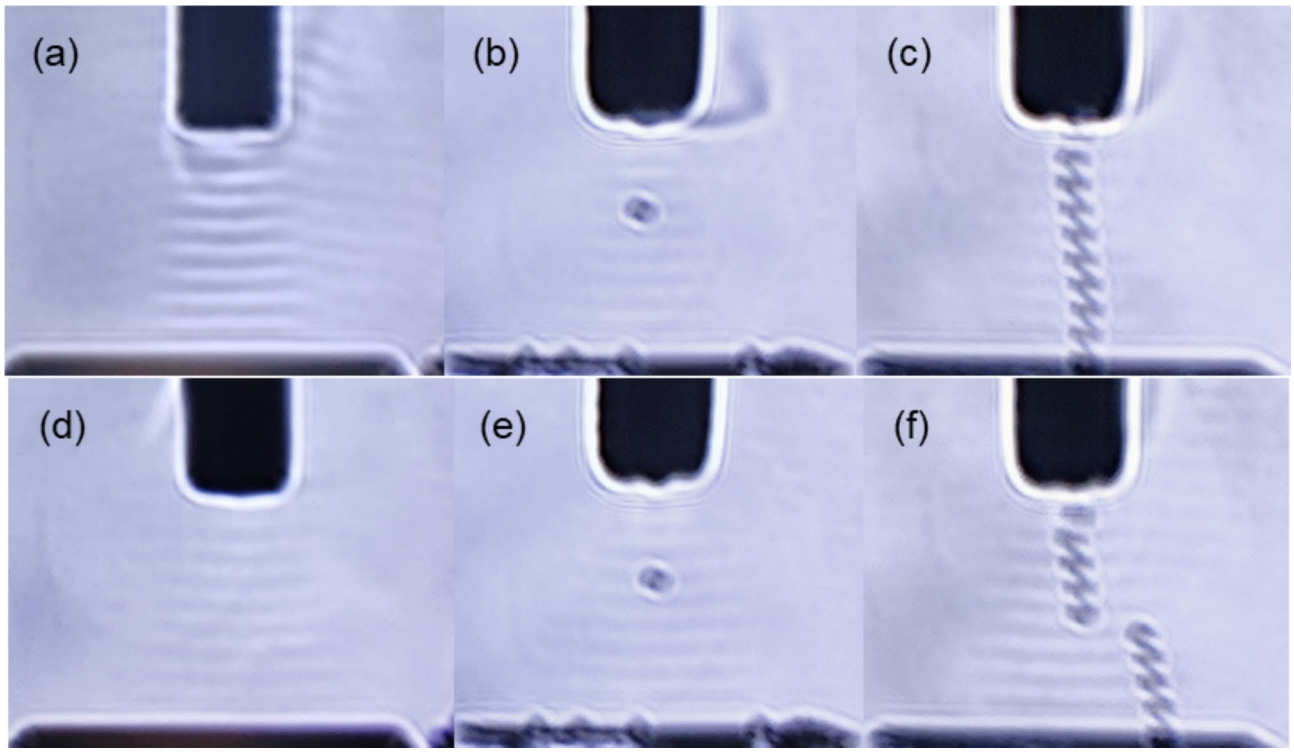

Fig. 2. Schlieren method to observe the change of the particle chain levitation bifurcation waveform. **a**–**c** At this time, the height of the resonant cavity is an integer multiple of the half-wavelength. The three figures are all standard standing wave acoustic field shapes. It can be seen that the waveform at this time is slightly narrower as a conical standing wave field. **d**–**f** When the height change increases by λ/8, the shape of the acoustic field of the three diagrams changes significantly. It can be seen that the lower part of the waveform is significantly widened and the bifurcation is obvious.

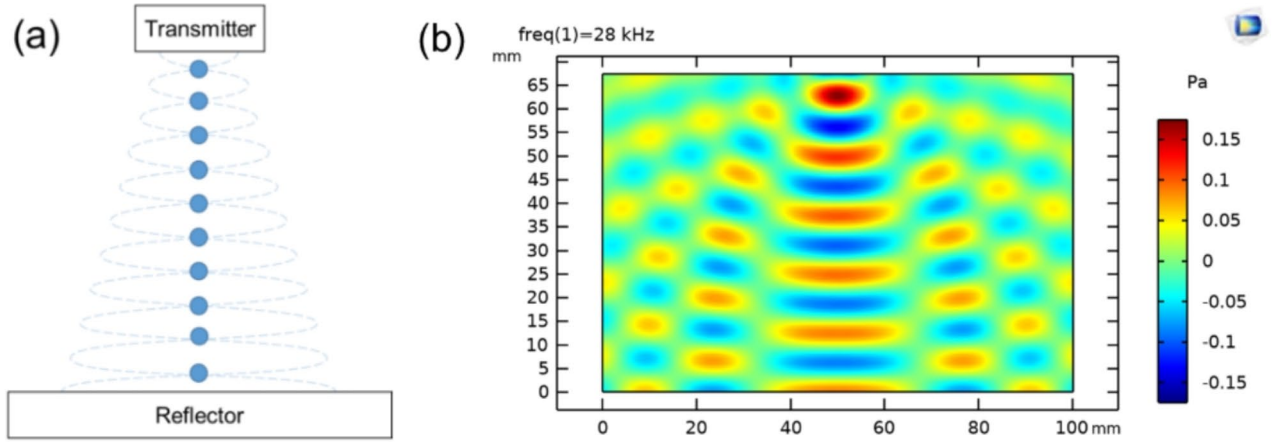

Fig. 3. Simulation of the particle chain in conical standing wave acoustic field. **a** Acoustic model diagram, because the transmitting end is much smaller than the reflecting end, forming a conical standing wave acoustic field. **b** COMSOL simulation results also show a conical standing wave acoustic field.

simplifies the equipment for acoustic levitation and acoustic manipulation, and can also achieve rapid and simple overall manipulation, targeted separation, and delivery of particle chains.

Subsequent research directions will continue to delve into other conditions and influencing factors for acoustic field bifurcation and jump, as well as the solution of acoustic potential energy and external force, and study the quantifiable manipulation performance of particle chains in this nonlinear composite field. Ultimately, the goal is to develop simplified equipment that can replace complex phased array equipment in specific situations.

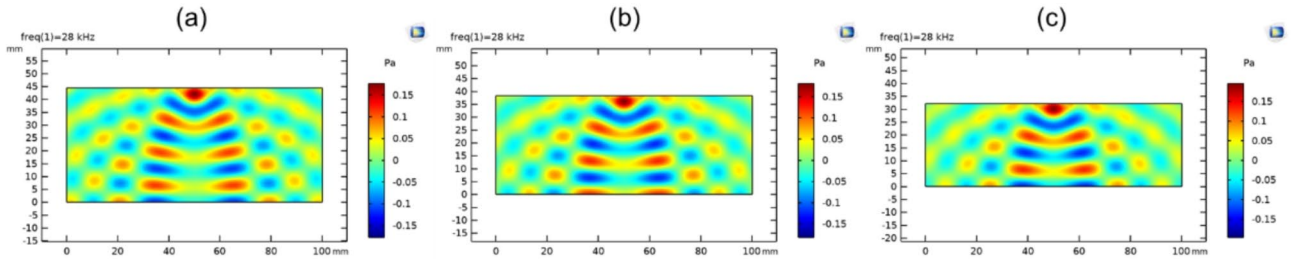

Fig. 4. Waveform simulation of each integer multiple half wavelength increasing λ/8. The resonant cavity height begins to appear obvious acoustic field bifurcation from 5.25 times the half wavelength. **a** Bifurcation simulation diagram of 7.25 times half wavelength. **b** Bifurcation simulation diagram of 6.25 times half wavelength. **c** Bifurcation simulation diagram of 5.25 times half wavelength.

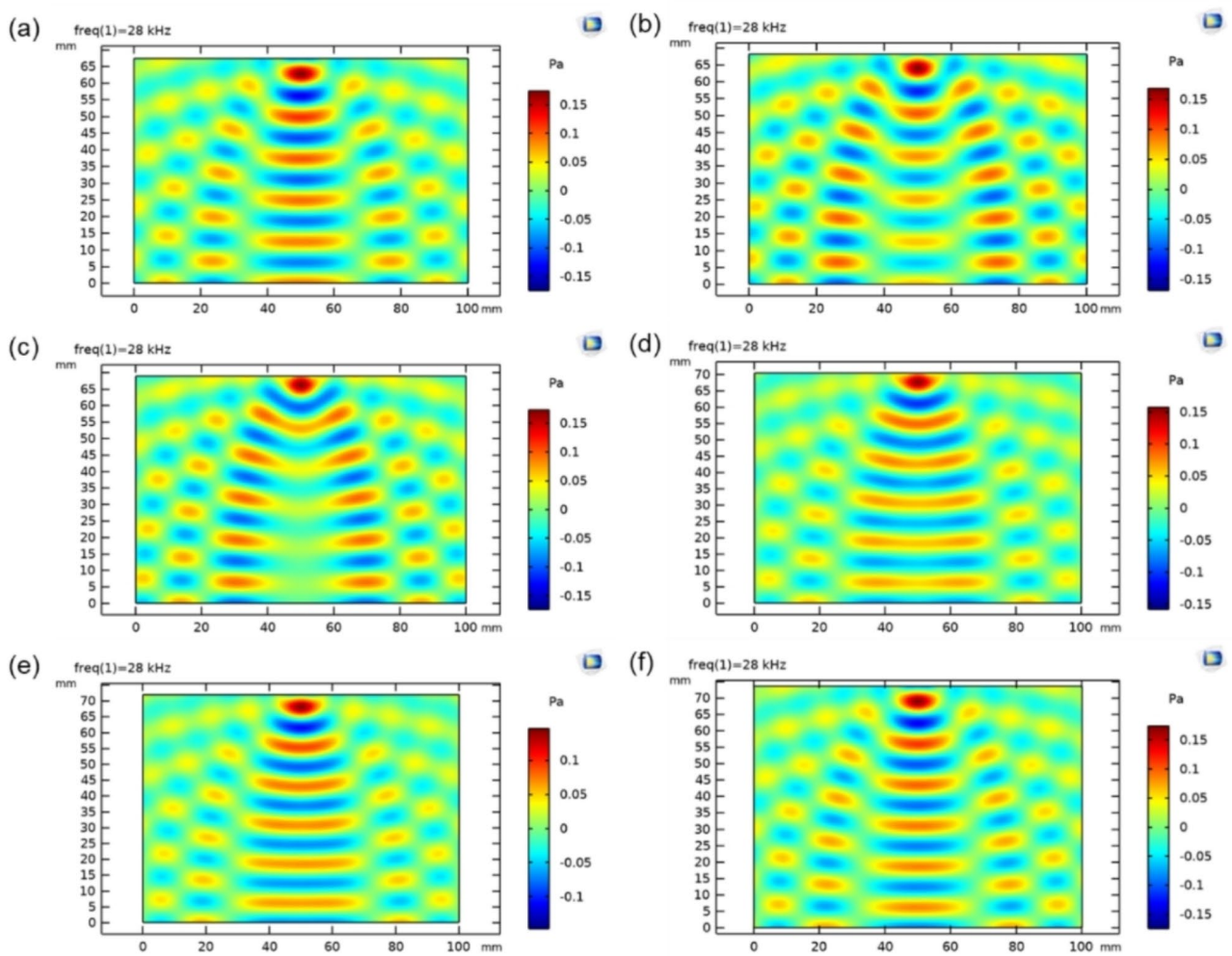

Fig. 5. Waveform simulation of the entire process in the 10-particle chain height changing from 11 to 12 times the half wavelength. **a** Simulation diagram of 11 times half wavelength. **b** Simulation diagram of 11.125 times half wavelength. **c** Simulation diagram of 11.25 times half wavelength. **d** Simulation diagram of 11.5 times half wavelength. **e** Simulation diagram of 11.75 times half wavelength. **f** Simulation diagram of 12 times half wavelength.

Methods

(1) Firstly, the motion equation of the particle chain is established, as shown in Fig. 8.

According to Newton 's second law, the vertical and horizontal equations of motion of the i-th particle can be expressed as[4,15]:

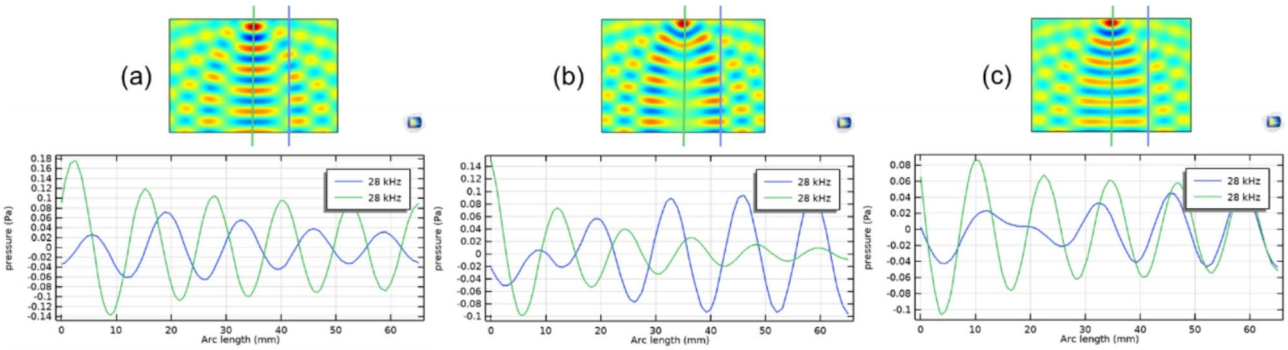

Fig. 6. Waveform comparison of the 10-particle chain height variation in the test. The green line represents the acoustic pressure intensity waveform curve at the center, and the blue line represents the acoustic pressure intensity waveform curve at the bifurcation side wave node. **a** Simulation acoustic pressure map of 11 times half wavelength. **b** Simulation acoustic pressure map of 11.25 times half wavelength. **c** Simulation acoustic pressure map of 11.5 times half wavelength.

$$\left.\begin{aligned} m_i\frac{d^2z}{dt^2} &= F_{zi} + F_{kzi} + G_i \\ m_i\frac{d^2y}{dt^2} &= F_{yi} + F_{kyi} \end{aligned}\right\} \tag{1}$$

where, m_i is the mass of the i-th particle, F_{zi} is the acoustic radiation force in the z-direction, F_{yi} is the acoustic radiation force in the y-direction is F_{yi}, F_{kzi} is the comprehensive external field force in the z-direction, and F_{kyi} is that of force in the y-direction.

At this time, the standing wave levitation is the initial stage, and the particle chain is stably suspended vertically in the standing wave field, which is consistent with the results of experimental Fig. 1a.

(2) Next, increasing the height of the resonant cavity, the standing wave field changes to a certain extent, and the lower end of the particle chain begins to bifurcate. As shown in Fig. 9, the particles at the lower end move horizontally.

The vibration displacement equations of the incident wave D_I and the reflected wave D_R in the standing wave acoustic field can be expressed as[23]:

$$\left.\begin{aligned} D_I &= A\cos(\omega t - kz) \\ D_R &= A\cos(\omega t + kz - 2kH + \pi) \end{aligned}\right\} \tag{2}$$

where, A is the amplitude, ω is the vibrational angular frequency, k is the wave number, H is the resonant cavity height.

According to the principle of acoustic wave superposition, the total vibration displacement D of particles formed by the superposition of incident wave and reflected wave can be expressed as:

$$D = D_I + D_R = A\cos(\omega t - kz) - A\cos(\omega t + kz - 2kH) \tag{3}$$

Derivation of the above formula can get the particle velocity u can be expressed as:

$$u = \frac{\partial D}{\partial t} \tag{4}$$

According to the basic equation of acoustics, the equation of motion of vibration velocity u and acoustic pressure p can be obtained as follows[2,10]:

$$\rho_0\frac{\partial u}{\partial t} + \frac{\partial p}{\partial z} = 0 \tag{5}$$

It can be concluded that the acoustic pressure p and the function expression $g(H)$ about the height of the resonant cavity can be expressed as[2,22,23]:

$$p = -2A\omega\rho_0 c_0 g(H)\sin\left(kz - \frac{kH}{2}\right)p(t) \tag{6}$$

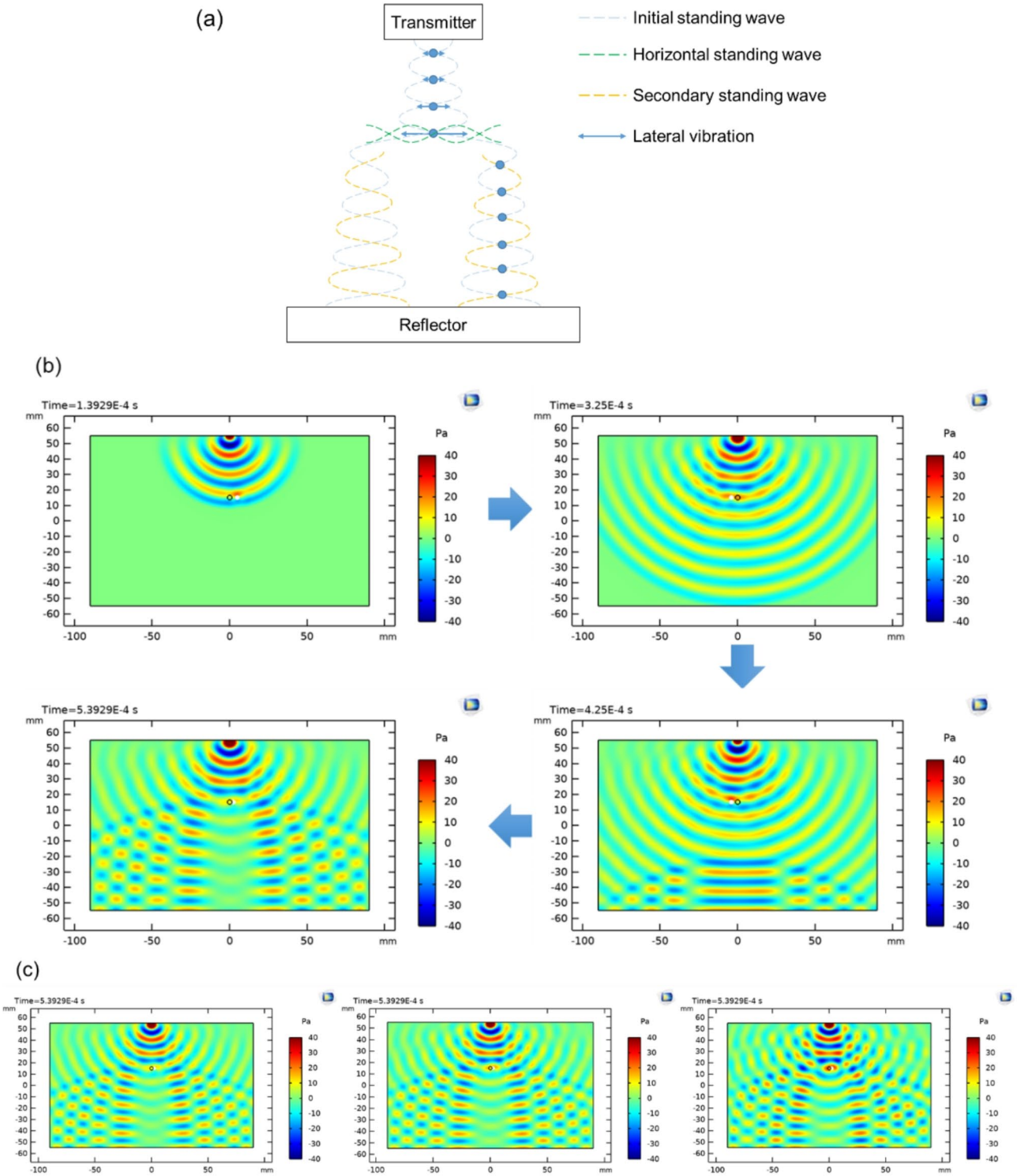

Fig. 7. Waveform simulation of secondary standing wave field and jump standing wave field. **a** The model diagram of secondary standing wave field and jump standing wave field. The lateral vibration of the fourth particle is the most intense, resulting in horizontal acoustic radiation force and lateral vibration, resulting in a jump standing wave field in the horizontal direction, making the particles jump quickly. **b** The dynamic simulation diagram of the secondary standing wave field and the jump standing wave field, the influence of the lateral vibration of the fourth particle on the conical standing wave field, and the waveform diagram of the generated jump standing wave field. **c** The influence diagram of the scattering amplitude size. The diagrams from left to right are respectively represented as 0 times the original amplitude, 0.1 times the original amplitude, and 0.3 times the original amplitude.

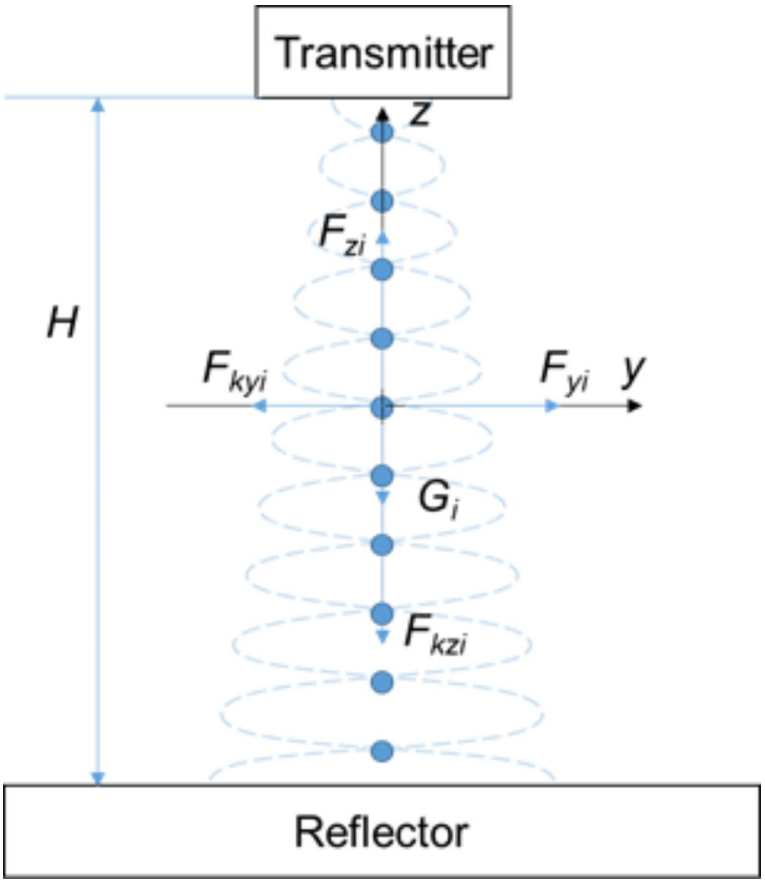

Fig. 8. Analysis of the particle chain levitation motion in a standing wave field. Analyze the two-dimensional motion model in vertical and horizontal directions. The ball represents the levitation position of the particle chain, and the dotted line represents the conical standing wave field.

$$\left.\begin{aligned} When\ i\ is\ an\ even\ number, g(H) = \frac{\cos\left[(i+1)\frac{kH}{2}\right]}{\cos\left(\frac{kH}{2}\right)}, p(t) = \cos\left(\omega t - \frac{i+1}{2}kH\right) \\ When\ i\ is\ an\ odd\ number, g(H) = \frac{-\sin\left[(i+1)\frac{kH}{2}\right]}{\cos\left(\frac{kH}{2}\right)}, p(t) = \sin\left(\omega t - \frac{i+1}{2}kH\right) \end{aligned}\right\}$$

where, ρ_0 is the static density of the medium, c_0 is the acoustic velocity of the medium.

It can be seen that the acoustic pressure p is affected by the height H of the resonant cavity. Ignoring the influence of gravitational potential energy, the equation of axial acoustic radiation force F_{zi} can be expressed as[4,10,23]:

$$F_{zi} = -\frac{20}{3}\rho_0 k A^2 \omega^2 g^2(H)\sin(2kz - kH) \tag{7}$$

Based on experimental observations and simulations, it is noted that the vibration of particles in the z-direction is negligible, so only the vibration in the y-direction is considered in subsequent analysis. By substituting $\theta = \partial y/\partial z$ into Eq. (7) from the differential basic equation, it can be concluded that[22,24]:

$$F_{yi} = F_{zi}\frac{\partial\theta}{\partial z} = F_{zi}\frac{\partial^2 y}{\partial z^2} \tag{8}$$

Taking Eq. (8) into Eq. (1), the horizontal motion equation can be obtained as follows:

$$m_i\frac{d^2y}{dt^2} - F_{zi}\frac{\partial^2 y}{\partial z^2} - F_{kyi} = 0 \tag{9}$$

Equation (9) is the horizontal motion equation of a single particle. The mechanical relationship of a single particle in the acoustic field can be equivalent to a nonlinear spring-mass model. Based on Eq. (9), a mathematical model

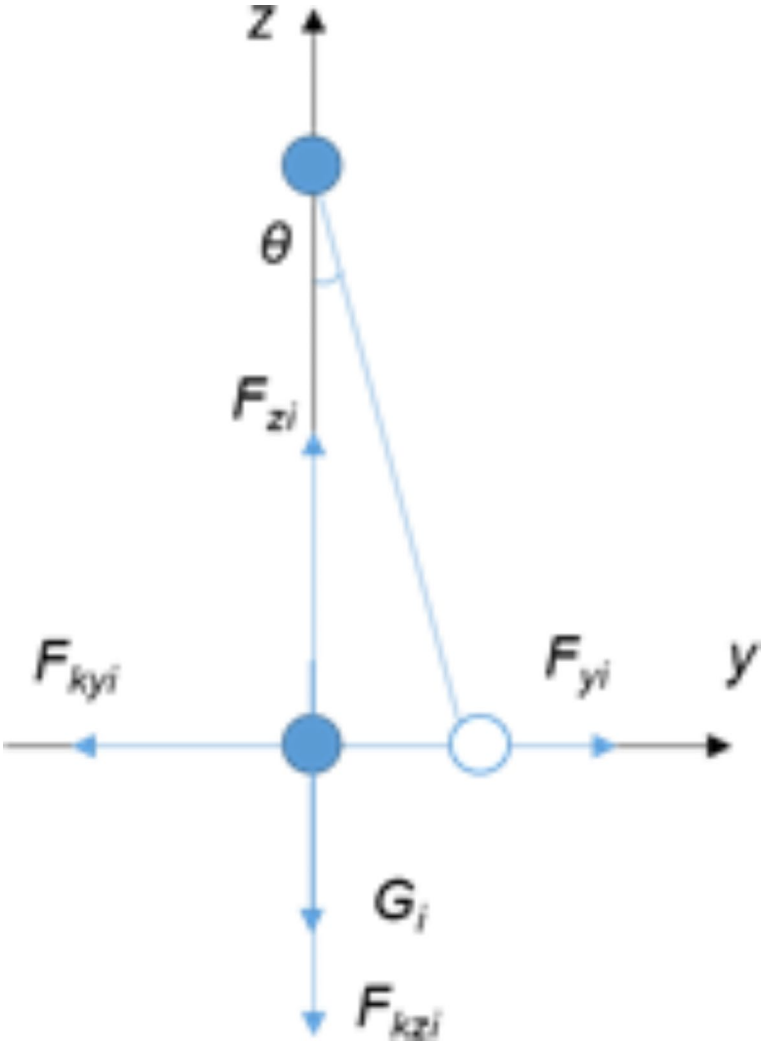

Fig. 9. Motion analysis diagram between bifurcated particles . The blue ball represents the initial levitation position, and the white ball represents the position after the bifurcation. At this time, an angle of motion will be generated.

of multiple particles connected by nonlinear springs is derived, and the Hamiltonian equation of the particle chain is introduced.

(3) These suspended particles can also be equivalently calculated by a two-dimensional particle chain connected by a nonlinear spring, as shown in Fig. 10.

The Hamiltonian equation of the particle chain can be expressed as[25]:

$$H = \frac{1}{2m}\sum_i y_i^2 + \frac{1}{2}\sum_i \left[\varphi\left(y_{i+1} - y_i\right) - \varphi\left(y_i - y_{i-1}\right)\right] + \sum_i V\left(y_i\right) \tag{10}$$

where, *V(y)* is the potential of the horizontal field, which is related to the comprehensive external field forces F_{kzi} and F_{kyi} in Eq. (1). The potential energy here can be used to derive the equivalent external field force.

Suppose the potential function $\varphi\left(y_i\right) = y_i^2$, the equation of motion of the i-th particle can be expressed as:

$$y = -\frac{\partial H}{\partial y_i} = \left(y_{i+1} - y_i\right) - \left(y_i - y_{i-1}\right) - V\left(y_i\right) \tag{11}$$

Through $y_i \to y\left(z, i\right)$, $\left(y_i - y_{i-1}\right) \to \partial y/\partial z$, the separation variable motion Eq. (11) is over to the continuous variable, which can be expressed as:

$$\frac{\partial^2 y}{\partial t^2} = \frac{\partial^2 y}{\partial z^2} - V'\left(y\right) \tag{12}$$

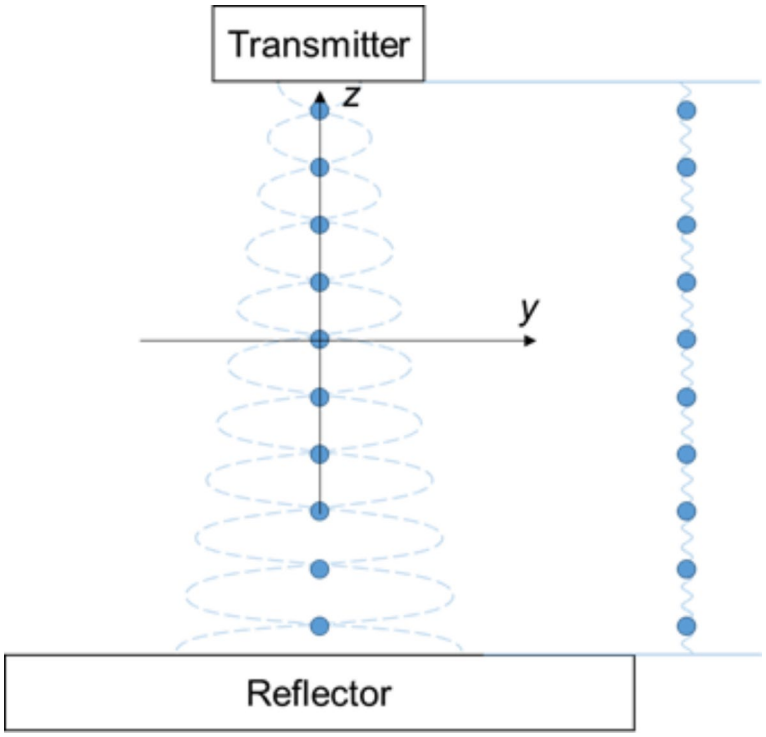

Fig. 10. The 2D particle chain equivalent diagram of nonlinear spring connection. On the left side is the levitation effect of the 10-particle chain in the conical standing wave field, which is equivalent to the movement of the 10-particle chain connected by the nonlinear spring on the right side.

When $V = \cos y$, the Eq. (12) can be expressed as:

$$\frac{\partial^2 y}{\partial t^2} - \frac{\partial^2 y}{\partial z^2} + \sin y = 0 \tag{13}$$

It can be seen that the Eq. (13) is the Sine-Gordon (SG) equation. According to the traveling wave solution of the SG equation, the kink solution of the SG equation can be obtained. By combining Eqs. (9) and (13) and substituting the parameters into the SG equation, the kink solution of the particle chain in this paper can be obtained.

(4) Next, the traveling wave method of SG equation is introduced. The general expression of SG equation is as follows[26,27]:

$$y_{tt} - c_0^2 y_{zz} + f_0^2 \sin y = 0 \tag{14}$$

Suppose $\xi = z - ct$, $y = y(\xi)$, then the SG equation can be expressed as:

$$\left(c^2 - c_0^2\right) \frac{d^2 y}{d\xi^2} + f_0^2 \sin y = 0 \tag{15}$$

Here only consider $c^2, c_0^2 (c^2, c_0^2$ similarly, omit), let $n^2 = f_0^2 / \left(c^2 - c_0^2\right)$, then the above equation is transformed into the same mathematical form of the motion equation of undamped single pendulum, it can be expressed as:

$$\frac{d^2 y}{d\xi^2} + n^2 \sin y = 0 \tag{16}$$

According to the single pendulum, the first integral can be obtained:

$$\frac{1}{2}\left(\frac{dy}{d\xi}\right)^2 + n^2 (1 - \cos y) = W \tag{17}$$

where, W is the integral constant, $W > 0$, let

$$z = \sin \frac{y}{2}, quadr^2 = \frac{W}{2n^2}$$

The Eq. (17) is transformed into

$$\left(\frac{dz}{d\xi}\right)^2 = n^2\left(1-z^2\right)\left(r^2-z^2\right) \tag{19}$$

As in the case of single pendulum, if $r^2<1$, the solution of the equation is an elliptic sine function solution.

$$z = \sin\frac{y}{2} = \pm r\mathrm{sn}\left[n\left(\xi-\xi_0\right), r\right] \tag{20}$$

This is the periodic solution (elliptic sine wave solution) of the SG equation, when c^2, c_0^2, where ξ_0 is an integral constant.

When $r\to 1$, Eq. (20) becomes a hyperbolic function solution.

$$\sin\frac{y}{2} = \tanh\left[\pm n\left(\xi-\xi_0\right)\right] \tag{21}$$

Using the definition of hyperbolic function, the above equation is transformed into:

$$e^{\pm n\sqrt{\xi-\xi_0}} = \sqrt{\frac{1+\sin\left(\frac{y}{2}\right)}{1-\sin\left(\frac{y}{2}\right)}} = \frac{1+\tan\left(\frac{y}{4}\right)}{1-\tan\left(\frac{y}{4}\right)} = \tan\left(\frac{y}{4}+\frac{\pi}{4}\right)$$

The Eq. (21) can be rewritten as follows:

$$y = -\pi + 4arc\tan\left[e^{\pm n(\xi-\xi_0)}\right] \tag{22}$$

Equation (22) is called the solitary wave solution of the SG equation: the positive exponential equation is called the kink wave, also known as the topological soliton; the negative exponent is called anti-kink wave, also known as anti-soliton[28].

(5) Eq. (9) is the horizontal motion equation of a single particle, and Eq. (13) is the horizontal motion equation of a particle chain. At this point, it can be found that the horizontal motion equations of both the single particle and the particle chain can be expressed as SG equations. The ultimate goal of deriving these two equations is to use the SG equation to explain the nonlinear motion behavior of the acoustic field, and to use the kink solution of the SG equation to explain the bifurcation and jump phenomena.

Comparing Eq. (9) and Eq. (13), Eq. (9) represents the motion of a single pendulum, which is consistent with the results of Fig. 1b. Equation (13) represents the kink solution of the SG equation, which can produce bifurcations and velocity solitons, which is consistent with the results of Fig. 1c. The kink solution and velocity soliton of the test principle are shown in Fig. 11.

From a theoretical perspective, the jumping critical point occurs at $\xi = \xi_0$, with its location given by $z_0 = \xi_0 + ct_0$, so it happens at a specific time and location, and under the experimental conditions of this paper, it happens to occur at the fourth particle.

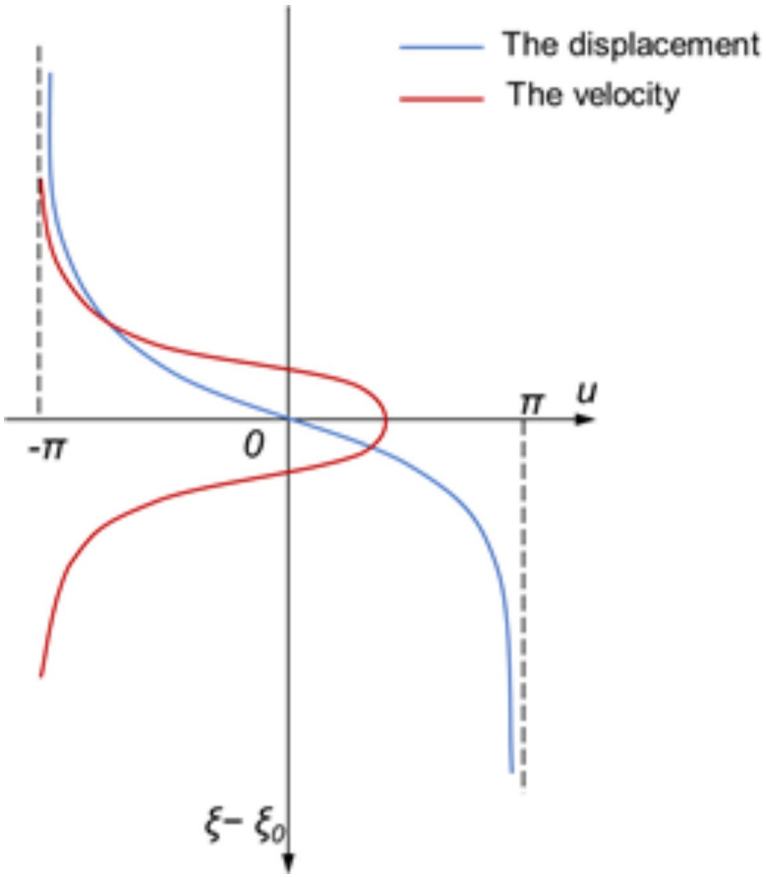

Fig. 11. The kink solution and velocity soliton of SG equation. The blue curve represents the displacement of the particles, which changes rapidly from the vertical levitation position to the bifurcation position. The red curve represents the velocity of the particle, from the stable state to the jump and then restore stability, forming a velocity soliton.

Data availability

All data generated or analysed during this study are included in this published article [and its supplementary information files].

Received: 26 May 2024; Accepted: 30 September 2024
Published online: 08 October 2024

References

1. H, B. E. Acoustic physics. Suspended by sound. *Nature***413**, 474–475 (2001).
2. Henrik, B. Acoustofluidics 7: the acoustic radiation force on small particles. *Lab. Chip* **12**, 1014–1021 (2012).
3. Yiannacou, K. & Sariola, V. Acoustic manipulation of particles in microfluidic chips with an adaptive controller that models acoustic fields. *Adv. Intell. Syst.* **5**, 2300058 (2023).
4. Thomas, L., Filip, P. & Andreas, N. Chip integrated strategies for acoustic separation and manipulation of cells and particles. *Chem. Soc. Rev.* **36**, 492–506 (2007).
5. Xiaoyun, D. et al. On-chip manipulation of single microparticles, cells, and organisms using surface acoustic waves. *Proc. Natl. Acad. Sci. USA* **109**, 11105–11109 (2012).
6. Daniele, F., Majid, N., Mirko, K., Aldo, F. & Dimos, P. Acoustophoretic contactless transport and handling of matter in air. *Proc. Natl. Acad. Sci. USA* **110**, 12549–12554 (2013).
7. J, X. W., D, C. C., J, L. Y. & B, W. Levitation of iridium and liquid mercury by ultrasound. *Phys. Rev. Lett.* **89**, 104304 (2002).
8. Mo, Z., Song, G., Shi, T. & Bolton, J. S. A poro-elastic model of sound propagation in granular materials. *J. Sound Vib.* **577**, 118337 (2024).
9. Dmitry, S. & Sergei, R. Particle levitation and control in midair using wideband ultrasonic waves. *Appl. Acoust.* **178**, 108004 (2021).
10. Liu, Q., Tang, Q. & Hu, J. A new strategy to capture single biological micro particles at the interface between a water film and substrate by ultrasonic tweezers. *Ultrasonics* **103**, 106067 (2020).
11. Yuyu, J. et al. Selective acoustic trapping, translating, rotating and orienting of organism from heterogeneous mixture. *IEEE Trans. Bio-med. Eng.* PP (2023).
12. Luke, C., Kai, M., Anthony, C. & Peer, F. & W, D. B. Acoustic hologram enhanced phased arrays for ultrasonic particle manipulation. *Phys. Rev. Appl.* **12**, 064055 (2019).
13. Peter, G. J. et al. Array-controlled ultrasonic manipulation of particles in planar acoustic resonator. *IEEE Trans. Ultrason. Ferroelectr. Freq. Control* **59**, 1258–1266 (2012).

14. W, S. M. & J, S. K. Validation of finite element analysis strategy to investigate acoustic levitation in a two-axis acoustic levitator. *Phys. Fluids.* **32** (2020).
15. Yaxing, W., Liqun, W. & Yajing, W. Study on particle manipulation in a metal internal channel under acoustic levitation. *Micromachines* **13**, 18–18 (2021).
16. Asier, M. et al. Holographic acoustic elements for manipulation of levitated objects. *Nat. Commun.* **6**, 8661 (2015).
17. Yang, I. H. & Kim, N. Comparisons of the acoustic radiation force of ultrasonic standing waves in half-wavelength and quarter-wavelength micro-resonators of cylindrical geometry. *Ultrasonics* **138**, 107267–107267 (2024).
18. Rudnick, I. Measurements of the acoustic radiation pressure on a sphere in a standing wave field. *J. Acoust. Soc. Am.* **23**, 633 (2005).
19. Chen, C., Guo, J. & Lin, S. Multi-mode coupled vibration analysis and radiation sound field investigation of a novel multidirectional piezoelectric ultrasonic transducer. *Ultrasonics* **138**, 107248 (2024).
20. Gerold, B., Rachmilevitch, I. & Prentice, P. Bifurcation of ensemble oscillations and acoustic emissions from early stage cavitation clouds in focused ultrasound. *New J. Phys.* **15**, 033044–033044 (2013).
21. Maxim, G. & Serge, G. F. W. Jump chaotic behaviour of ultra low loss bulk acoustic wave cavities. *Appl. Phys. Lett.* **105**, 063501–063501 (2014).
22. Fangtao, X., Yegao, Q. & Guang, M. Numerical analyses of nonlinear acoustic wave radiation behaviors of vibrational objects immersed in infinite fluid. *Mech. Syst. Signal Process.* **163**, 108176 (2022).
23. Longfei, J. *Simulation and experiment on the characteristics of an acoustic field by contraposition type transducer array*. Master of Engineering thesis, Harbin Institute of Technology (2017).
24. Zhou, K. *The study of tool lateral vibration in micro USM*. Dalian University of Technology (2017).
25. M D, J. E. Nonlinear wave transmission in harmonically driven hamiltonian Sine-Gordon regimes with memory effects. *Chaos Solitons Fractals* 110362 (2020).
26. Shou-xian, S. Nonlinear vibrations, nonlinear waves and jacobian elliptic functions. *Coll. Phys.* 3–7. https://doi.org/10.16854/j.cnki.1000-0712.2004.02.019 (2004).
27. Majid, W. A. New integrable (2 + 1)-dimensional Sine-Gordon equations with constant and time-dependent coefficients: multiple optical kink wave solutions. *Optik* **216**, 164640 (2020).
28. Huiyang, Z. & Yonghui, X. Persistence of kink and anti-kink wave solutions for the perturbed double Sine-Gordon equation. *Appl. Math. Lett.* **141**, 108616 (2023).

Acknowledgements

This work has been supported by the National Natural Science Foundation of China under Grant No.52175460.

Author contributions

Y. W. and L. W. contributed conceptualization, methodology and validation; Y. W. contributed software analysis, investigation, writing, review and editing; L. W. contributed project administration and funding supported; Y. W., G. W. and J. W. contributed experiment; L.Z. and H.W. contributed supervision and resources. All authors have read and agreed to the published version of the manuscript.

Declarations

Competing interests

The authors declare no competing interests.

Additional information

Correspondence and requests for materials should be addressed to Y.W.

Reprints and permissions information is available at www.nature.com/reprints.

Publisher's note Springer Nature remains neutral with regard to jurisdictional claims in published maps and institutional affiliations.